

HRTEM and EELS study of screw dislocation cores in SrTiO₃

Zaoli Zhang, Wilfried Sigle, and Wolfgang Kurtz

Max-Planck-Institut für Metallforschung, Heisenbergstraße 3, D-70569 Stuttgart, Germany

(Received 8 May 2003; revised manuscript received 8 October 2003; published 5 April 2004)

A [100] twist low-angle grain boundary in SrTiO₃ was systemically studied by means of conventional transmission electron microscopy, high-resolution transmission electron microscopy (HRTEM), lattice distortion analysis, and electron energy-loss spectroscopy (EELS). A dislocation network is formed in the grain boundary by two sets of $a\langle 100 \rangle$ screw dislocations. HRTEM images show that the image contrast in the core region is different from that in the surrounding bulk. Image analysis reveals that compared with an ideal screw dislocation the dislocation core is expanded, probably due to both surface relaxation and a reconstruction of the core. The EELS spectra show a small increase of the Ti/O ratio but no significant change of the Sr/Ti ratio in the core region. From the increase of the Ti/O ratio it is concluded that the dislocation cores are oxygen deficient, which may be responsible for the expansion of the core. Ti $L_{2,3}$ EELS spectra show a reduction of Ti in the screw dislocation cores as well as a reduced crystal field splitting, both of which are in accordance with a loss of oxygen.

DOI: 10.1103/PhysRevB.69.144103

PACS number(s): 61.72.Mm, 82.80.Pv, 61.72.Ff

I. INTRODUCTION

SrTiO₃ with a perovskite structure is one of the most important oxides, used as a dielectric material in capacitors as well as a substrate in epitaxially grown heterostructures.¹ This is confirmed by the large number of recent publications in this field. Among the investigations focusing on the electronic and atomic structure,^{2–4} various special types of grain boundaries in particular have received considerable interest since such interfaces or grain boundaries play an important role in various applications. The combination of *Z*-contrast imaging, high-resolution transmission electron microscopy (HRTEM), electron energy-loss spectroscopy (EELS), and *in situ* heating provides an experimental tool with unparalleled spatial resolution, energy resolution, and chemical sensitivity to investigate the atomic scale structure, composition, and dynamics.^{5–8}

Defects studied in bulk and thin film SrTiO₃ were recently reported by several authors. Dislocations were studied by Nishigaki *et al.*⁹ and Mao and Knowles¹⁰ after high-temperature deformation and by Matsunaga and Saka¹¹ after deformation at room temperature introduced by Vickers indentation. Misfit dislocations in thin films were studied by Qin *et al.*¹² Initiated by the surprising plastic behavior¹³ and the strong blocking effect for charge transport in impedance measurements,¹⁴ recently the atomic scale structure and chemistry of a perfect edge dislocation core and a dissociated edge partial dislocation core in SrTiO₃ were systematically investigated by HRTEM and high-spatially-resolved EELS.^{15,16} It was shown that the electronic and atomic structure of dislocation cores in SrTiO₃ is closely correlated with these properties. Moreover, the detailed dislocation analysis performed on the deformed SrTiO₃ single crystal indicated that the $a\langle 100 \rangle$ screw dislocation, which should have the lowest line energy in the perovskite lattice, is not involved in the surprising mechanical behavior. With the present analysis we try to shed some light on this phenomenon.

Experimental studies of screw dislocation cores have been

reported up to now for GaN,^{17,18} molybdenum,^{19,20} and gold and iridium.^{21,22} The results indicate a correlation of the screw dislocation core structure with the electrical properties¹⁸ and the plasticity.^{19–22} A general difficulty of studies by HRTEM is that the displacement field has components only along the dislocation line, which is also the observation direction. Therefore the contrast is usually almost identical to the perfect crystal lattice. This “projection problem” is not present for analytical TEM studies, which therefore contain important additional information. Despite this fact no such analytical studies of screw dislocation cores have been reported yet except in GaN.¹⁷ A further motivation for the present study is the more general question about the structure of screw dislocations in materials with (partially) ionic bonding.

II. EXPERIMENTAL PROCEDURES

A SrTiO₃ bicrystal with a [100] low-angle twist grain boundary of $\sim 1^\circ$ twist angle was produced by diffusion bonding from two undoped SrTiO₃ crystal platelets (purchased from Crystal GmbH, Berlin) in UHV.^{23,24} The sample size was $10 \times 10 \times 0.8$ mm³, with the grain boundary parallel to the large sample faces. The surfaces to be bonded were polished carefully. For the detailed procedure we refer to a former paper.¹⁵ The exact twist angle was measured to be 0.7° from Kikuchi patterns recorded on both sides of the grain boundary.

The sample preparation procedure for TEM and HRTEM was achieved using a standard technique as described in a former paper.¹⁶ In addition, a final ion polishing with low-energy Ar ions (0.5 keV) was done using a Technoorg Linda ion mill. This is especially important to avoid radiation damage and reduce the thickness of disordered layers on the two surfaces of the TEM specimen.

A Philips CM20 microscope operated at 200 kV with a point resolution of 0.27 nm was used to get conventional diffraction contrast images. HRTEM phase contrast images were acquired parallel to the $\langle 100 \rangle$ dislocation line using the

JEOL ARM 1250 microscope operated at 1250 kV with a point resolution of 0.12 nm.

HRTEM simulations were done by the multislice method using the electron microscopy software package EMS.²⁵ The microscope parameters used in the simulations included a spherical aberration coefficient of $C_s = 2.7$ mm, a Gaussian spread of focus of 11 nm, and a semiangle of the beam divergence of 0.3 mrad. The supercell for the image simulation has the dimension $3.5145 \times 3.5145 \times 0.3890$ nm³ (nine unit cells of SrTiO₃) and was sampled with 512×512 points.

For EELS experiments, a dedicated scanning transmission electron microscope (VG HB 501 UX, Vacuum Generators) was used. The microscope was operated at 100 keV. It is equipped with a cold field-emission gun, an energy dispersive x-ray spectrometer (Noran), and an electron energy-loss spectrometer (Gatan UHV Enfina 766). The energy resolution in EELS, as measured by the full width at half maximum of the zero-loss peak, was 0.7 eV. At the microscope setting used, the electron probe size is smaller than 0.5 nm. EELS spectra were recorded with a dispersion of 0.1 eV/channel, which allows one to simultaneously acquire the Ti $L_{2,3}$ edge and the O K edge and to determine peak positions with high accuracy. For the acquisition of the Sr $L_{2,3}$ edge at an energy loss of 1940 eV a dispersion of 0.7 eV/channel was used. The total acquisition time for the Sr L edge was 20 s and of the Ti L and O K edges 15 s. Spectra from eight individual cores were recorded. The energy scale for the EELS spectra was calibrated by setting the first white line of Ti $L_{2,3}$ to 456 eV or of Sr $L_{2,3}$ to 1940 eV. For this reason the energy shifts stated below denote *relative* energy shifts. The convergence and collection semiangles were both 6.5 mrad. All data shown here were corrected for dark current of the charge-coupled device array and detector gain variation. The spectrum acquisition and processing were done using the same procedures as described in a previous paper.¹⁶ A power law function and the Hartree-Slater model were used to remove the background and to quantify the composition. The energy ranges for the quantification and the background removal were 453.9–488.2 eV and 419.6–444.1 eV for the Ti $L_{2,3}$ edge, 528.8–557.5 eV and 501.5–521.8 eV for the O K edge, and 1935.1–2089.8 eV and 1790.2–1914.8 eV for the Sr $L_{2,3}$ edge.

Local information from the dislocation core can be obtained by directly placing the electron beam in the center of the core. Owing to the difficulty of locating the exact core precisely, we measured EELS spectra from a small rectangular area of 6×8 nm² containing one dislocation core (“area measurement”). In this case specimen drift can be corrected manually during the acquisition since the image and EELS spectra are recorded simultaneously. Alternatively, we acquired a set of 5×5 spectra within a 3×3 nm² matrix containing an individual core (“EELS mapping”). This technique allows us to get spectra from areas containing only a few atom columns around the dislocation core. The separation between neighboring measurements was about 0.6 nm. The integration time for each spectrum was 3 s. In general, one or two spectra were found to be different from the others, and we

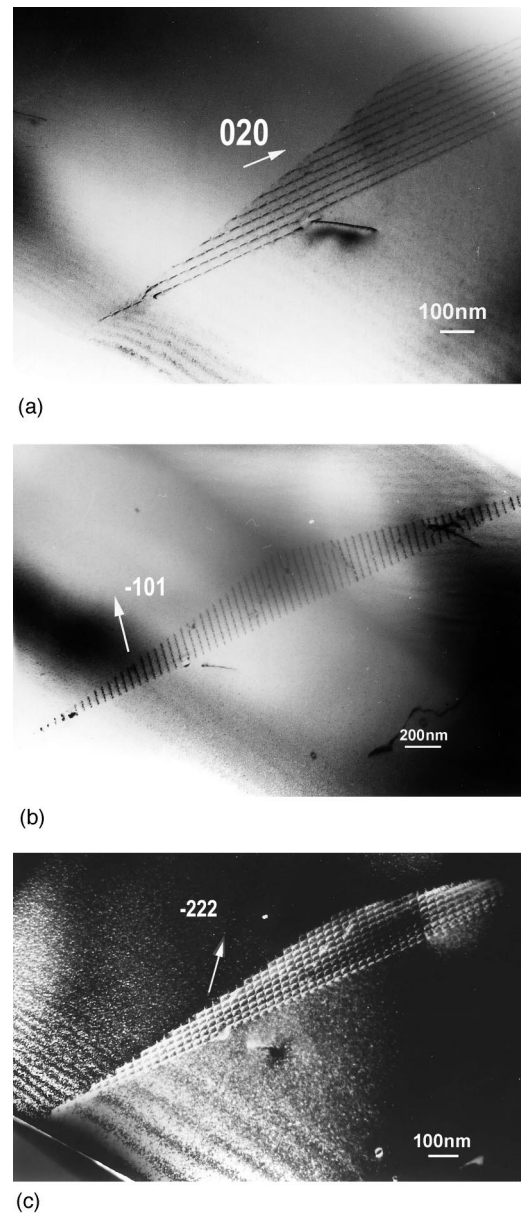


FIG. 1. Bright field image using (a) $\mathbf{g}=020$ and (b) $\mathbf{g}=\bar{1}01$ diffraction vectors. The two sets of the dislocation network are visible. The whole network is shown in the dark field image using $\mathbf{g}=\bar{2}22$ (c). The beam direction is always close to $[101]$.

then assigned this/these as the dislocation core specific spectrum/spectra.

III. RESULTS

A. Conventional TEM

Figure 1 is a low-magnification diffraction contrast image of the twist grain boundary. From the invisibility criterion $\mathbf{g} \cdot \mathbf{b} = 0$, where \mathbf{g} is the diffraction vector and \mathbf{b} the Burgers vector, we found that the dislocation network consists of two sets of $\langle 100 \rangle$ screw dislocations. Figures 1(a) and 1(b) are bright field images using $\mathbf{g}=020$ and $\bar{1}01$, which show the two sets of parallel screw dislocations. The dark

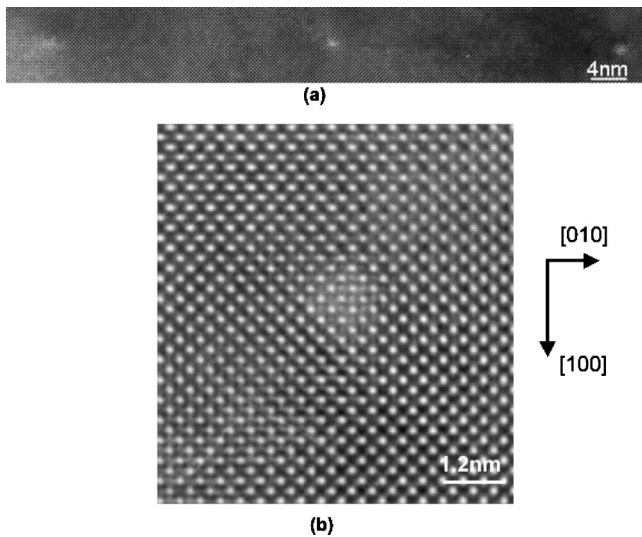


FIG. 2. (a) HRTEM image of the 0.7° 100 symmetrical twist grain boundary showing three dislocation cores. (b) Enlarged image of one screw dislocation core. Note the different contrast in the core as compared to the bulk region. Slight distortions are visible when viewing along atom rows under a glancing angle.

field image [Fig. 1(c)] using $\mathbf{g}=\bar{2}22$ presents a well-defined dislocation network. The beam direction is close to the $[101]$ zone axis. From the images it can be seen that within very thin areas around the edge only the set of short screw dislocations with line direction perpendicular to the foil surfaces is present.

B. HRTEM and image processing

Figure 2(a) is a HRTEM image of the low-angle $[100]$ twist grain boundary recorded with a defocus value of -60 nm. The image shows that the misorientation between the two crystals leads to the formation of a regular array of crystal imperfections separated by regions of perfect lattice.

The pure twist grain boundary is composed of screw dislocations, the average spacing of which is 31.2 ± 0.8 nm from the high-resolution image. According to Frank’s formula the misorientation angle can be determined to be $(0.72 \pm 0.02)^\circ$, which is in agreement with the experimental value from the Kikuchi pattern.

Although the enlarged image of the dislocation core region [in Fig. 2(b)] shows an almost perfect lattice, close inspection shows that slight distortions are present around the core, which can be seen by viewing under a glancing angle. Moreover, some blurred contrast is present around the core as well as some additional weak bright points as compared with the regular lattice.

Image simulations have been performed in order to investigate whether the image maxima in Fig. 2 correspond to the positions of atom columns. The atomic model [Fig. 3(a)] was generated from the anisotropic elastic displacement field using the program GENESIS written by Vitek. A simulated HRTEM image based on this structure model is shown in Fig. 3(b) for the experimental conditions (defocus -60 nm,

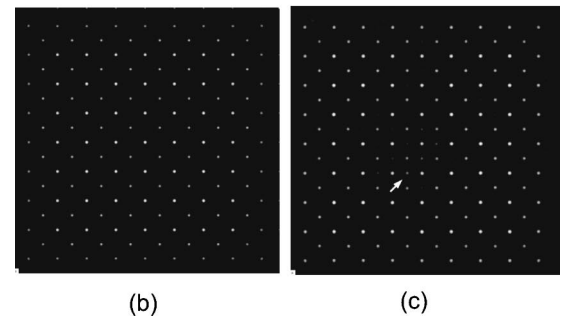
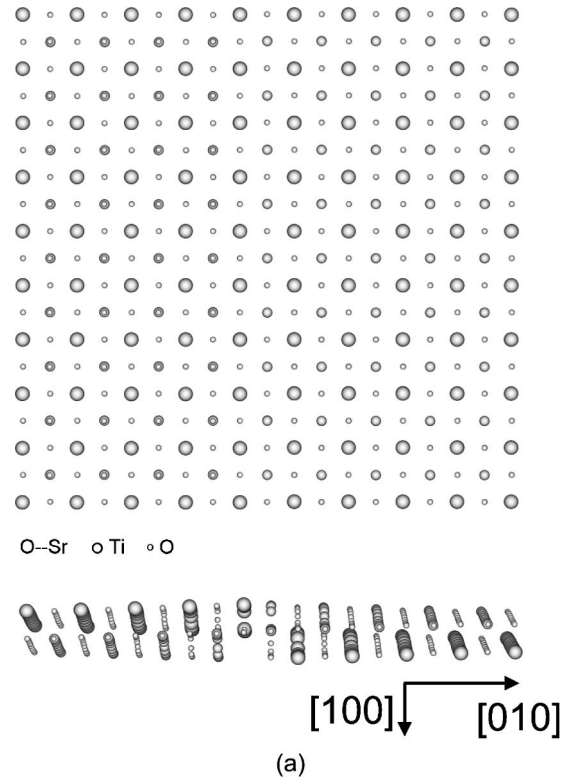


FIG. 3. (a) An atomic model of a screw dislocation core generated by the GENESIS program which is based on anisotropic elasticity theory. (b) The simulated image based on the above atomic model using the experimental conditions. (c) The simulated image using the atomic model modified by adding the displacements of atom columns shown in Fig. 4.

thickness 5.47 nm). By superimposing the atom column positions from the atomic model on the simulated image, it can be seen that under these imaging conditions bright contrast corresponds to the Sr and Ti–O atom column positions. Oxygen atom columns are invisible. Note, however, that the additional contrasts in the interstitial regions near the core in the experimental image are not present in this simulation. This will be discussed later.

In order to map the displacement field in the core region the HRTEM image was processed using the software package LADIA.²⁶ A reference lattice from the nearby perfect bulk was constructed from the positions of the bright dots in a circular ring of radius between about 2.8 and 3.6 nm, the center of which is located in the center of the dislocation core. This perfect lattice was then extended into the core

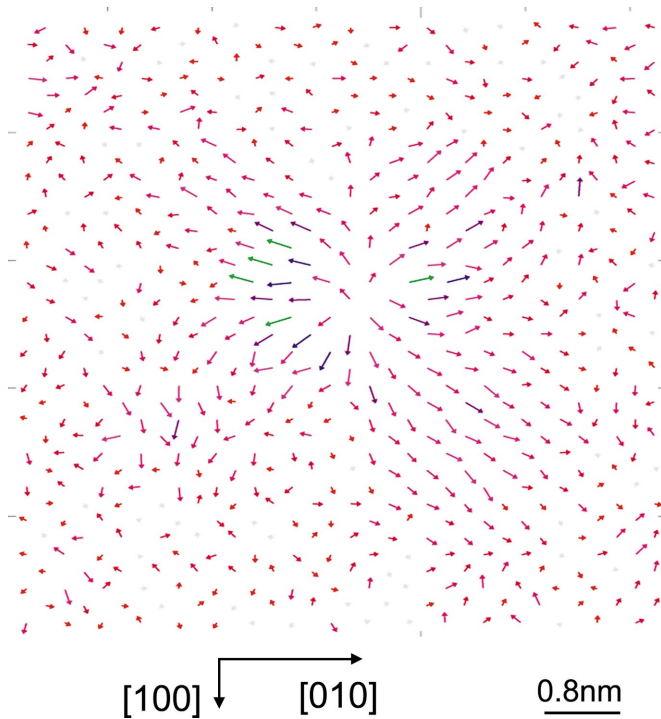


FIG. 4. (Color) Displacement map of the screw dislocation core shown in Fig. 2(b). The arrows show that the positions of atom columns in the core deviate from a perfect reference lattice. The arrows are shown not in red if their length exceeds a certain value. The displacements extend preferably along the $\langle 110 \rangle$ directions, leading to a fourfold symmetry of the core structure.

region. The deviation of this perfect lattice from the real lattice gives us the displacement field projected along the $\langle 100 \rangle$ observation direction. The displacements are displayed as arrows which connect the position of each reference lattice point with the center of the nearest image dot (Fig. 4). One can clearly see a shift of atom columns away from the core position with a maximal shift of 25 pm. Note that the magnitude of the displacements in the core region is significantly higher than the scatter of the displacements remote from the core region. A typical detection limit for displacements measured by this technique is 10 pm, which mainly depends on the sampling rate during the image processing.

The shift of atom columns away from the core corresponds to an expansion of the core as compared to an ideal screw dislocation. Close inspection shows that the spatial extension of the relaxations is more pronounced along the four $\langle 110 \rangle$ directions than along the $\langle 100 \rangle$ directions, i.e., the dislocation core shows a fourfold dissociation.

C. EELS analysis

1. Area measurement

From the quantification of the core and bulk spectra we obtained average compositions of eight cores shown in Fig. 5. It can be seen that in the screw core the Ti/O ratio is higher than in the bulk whereas the Sr/Ti ratio shows almost no change.

A core specific EELS spectrum can be extracted by applying the spatial difference technique.^{27,28} This technique can easily be applied to the spectra from area measurements because these spectra have a high signal-to-noise ratio. We assumed that the dislocation core specific signal originates from atoms located up to the second-nearest neighbor from the core. This means that the EELS spectrum acquired in the core region contains about 33% real core signal. Using this factor, we obtain the core specific signal shown at the bottom of Fig. 6. The difference spectrum shows a reduced crystal field splitting by 0.4 ± 0.1 eV in the dislocation core region. A chemical shift of the Ti $L_{2,3}$ edge of 0.3 ± 0.1 eV toward lower energy loss is observed. EELS quantification shows that the Ti/O ratio in the dislocation core is increased by about 13 ± 5 %.

2. EELS mapping

Figure 7 shows the Ti $L_{2,3}$ and O K spectra from an individual dislocation core and from the nearby bulk. Here, the bulk spectrum was obtained by adding five bulk spectra around the core. No obvious change in the O K edge was found. By careful inspection one can see a slight decrease of the ligand field splitting by 0.25 ± 0.1 eV in the Ti $L_{2,3}$ edge as indicated by dotted lines. The e_g and t_{2g} peaks are narrower in the bulk region [Fig. 7(b)]. These features can be seen more easily from the two smoothed spectra that were obtained by applying a 0.8 eV low-pass filter. Following the

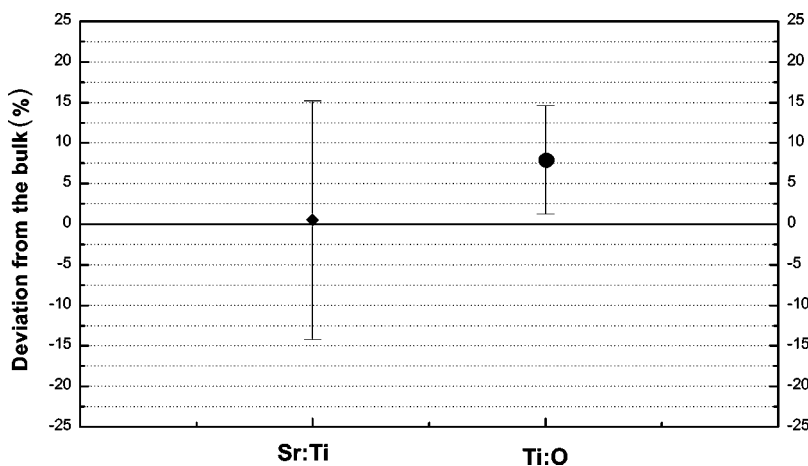
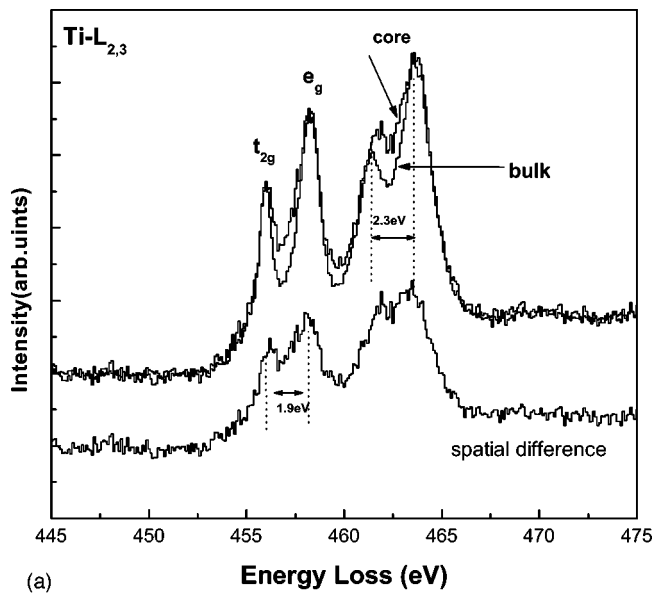
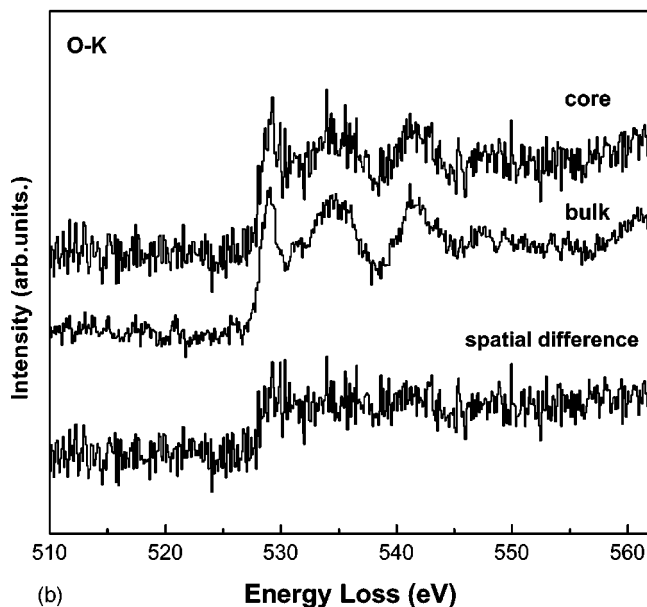


FIG. 5. The average composition (Sr/Ti and Ti/O ratios) of eight screw dislocation cores obtained by area EELS measurements.



(a)



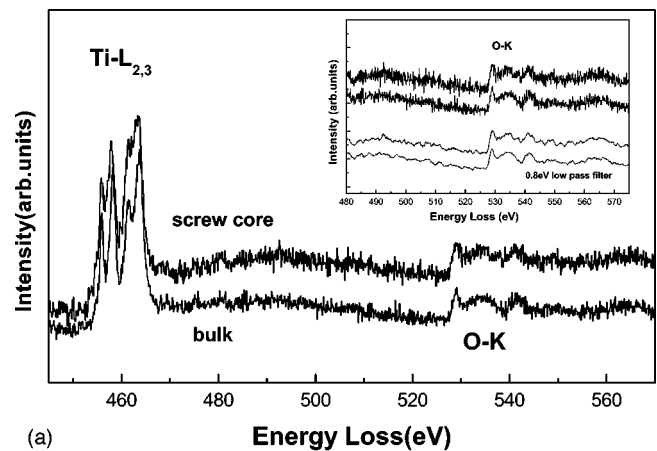
(b)

FIG. 6. (a) Ti $L_{2,3}$ edge obtained by an area measurement. The core specific ELNES is shown at the bottom and was obtained by the spatial difference method. The edge shows a decrease of the crystal field splitting. (b) O K spectrum obtained by an area measurement. It probably shows a slight change of the second peak.

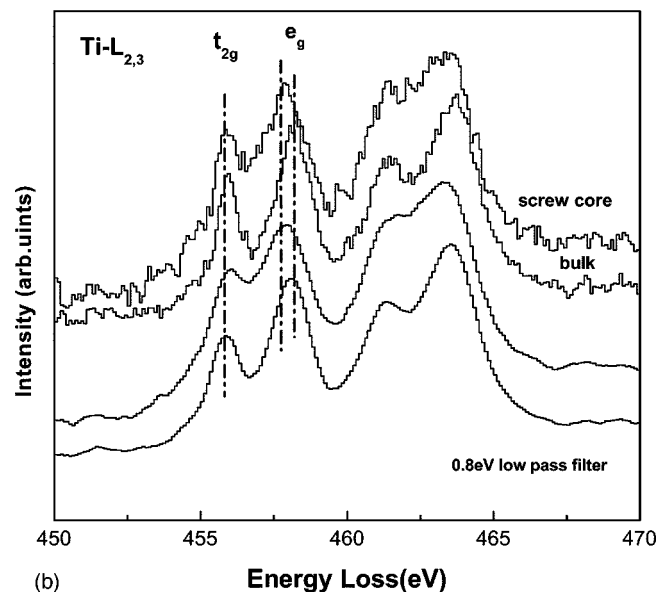
technique of Pearson *et al.*²⁹ an increase of the L_3/L_2 ratio by 22% and a decrease of the e_g/t_{2g} intensity ratio by 12% is found in the core. EELS quantification shows an increase of the Ti/O ratio by $3.9 \pm 9.4\%$ in the core as compared to the bulk. We could not clarify why this value is lower than the one obtained from the area measurements. The opposite should be expected since in the mapping we are probing smaller areas. In any case, we find consistently an increase of the Ti/O ratio.

IV. DISCUSSION

From Fig. 1 it can be seen that in the thicker regions the grain boundary is composed of two perpendicular sets of



(a)



(b)

FIG. 7. (a) Two spectra extracted from the EELS map, one from a screw dislocation core and the other from the surrounding bulk region, which is an average of several bulk spectra. (b) Enlargement of the Ti $L_{2,3}$ edge showing a significant narrowing of e_g and t_{2g} peaks in the L_3 edge. The O K edge shows no pronounced changes.

$\langle 100 \rangle$ screw dislocations. A complication for the analysis of HRTEM and EELS data could arise from the crossing of these dislocations. However, within the thin areas which were used for EELS and HRTEM, only a single set of dislocations is left. Obviously the dislocations running almost parallel to the specimen surface have glided to the surfaces in these regions. This is also supported by the fact that no strain contrast of such dislocations was visible in the HRTEM images.

The simulated image from a screw dislocation calculated from anisotropic elasticity theory [Fig. 3(b)] shows no additional contrast in the dislocation core. However, the experimental image exhibits blurred contrast in the core region as well as some additional weak bright points. These contrast variations show that there must be a structural change in the core. It is rather unlikely that this is due to a non-straight dislocation since any kink would increase the line energy of a screw dislocation. We rather believe

that the contrast originates from a combination of surface relaxation and a reconstruction of the core leading to small edge components due to the small foil thickness as has been observed in molybdenum.¹⁹ It is clear from Ref. 19 that surface relaxations can significantly contribute to the HRTEM image contrast of screw dislocations. For a thin molybdenum foil it was demonstrated that the surface relaxation results in a movement of atom columns away from the center of the core. This is very similar to the present results. However, it is interesting to note that the additional contrast is present both in the thinnest and in thicker specimen regions (Fig. 2). If this contrast was simply due to surface relaxation effects it should become weaker in thicker areas. This strongly suggests that apart from the surface relaxation additional relaxations occur in the screw core. The strain map (Fig. 4) shows that the relaxation corresponds to an expansion of the core, probably with a fourfold symmetry. This symmetry could be interpreted such that the core contains four small $\langle 110 \rangle$ edge components. It is well known that the strong increase of the flow stress in body-centered metals is due to the threefold dissociation of the $a\langle 111 \rangle$ screw dislocation core which needs considerable thermal activation to make glide possible. In a similar way the fourfold dissociation observed here is likely to prevent the motion of $a\langle 100 \rangle$ screw dislocations in the perovskite lattice. We suppose that this is the reason why this type of dislocations is not observed after plastic deformation of SrTiO₃.

In order to see whether the core expansion is responsible for the observed contrast variations in the HRTEM image we performed the following analysis. Starting from the displacement map we used the displacement for each atom column and transferred this value to the corresponding column in the atom model used for the image simulations. Since under these imaging conditions oxygen columns are invisible the shifts are added only to the Sr and Ti–O atom columns. Figure 3(c) shows the calculated image based on this atomic model. It can be seen that additional weak contrast, which is indicated by an arrow, is present in the core region at the same positions as in the experimental image. This additional contrast does not exist in the calculated image from the anisotropic elasticity theory [Fig. 3(b); see the same positions as those in Fig. 3(c)]. Although the magnitude and shape is not exactly the same as in Fig. 2(b) this result shows that this type of contrast probably originates from the expansion of the core. Atomistic simulations would be clearly desirable to find out the origin of these contrast variations and to distinguish thin foil effects from real core reconstructions. However, owing to the complex ionic/covalent nature of the interatomic interactions in SrTiO₃ such simulations are extremely difficult and have not been reported up to now.

We now turn to the question if chemical effects could contribute to the core expansion. From the EELS area measurement (Figs. 5 and 6) it can be seen that the Sr/Ti ratio is almost constant while the Ti/O ratio is reduced compared with the bulk. This means that there is an oxygen deficiency in the core. In the perovskite structure Ti atoms are surrounded by an oxygen octahedron. Since adjacent octahedra

share one corner, two Ti atoms are always separated by an oxygen atom. A removal of oxygen will therefore inevitably lead to a repulsion of the two positive Ti ions and this could be the reason why the atom columns near the core are shifted away from the core.

The energy-loss near edge structure (ELNES) of absorption edges gives information on the site and symmetry projected unoccupied density of states near the Fermi level and is performed to gain insight into the electronic structure of the materials. The correlation of the ELNES of the Ti $L_{2,3}$ and O K edges with structural features in SrTiO₃ was reviewed in a previous paper.¹⁵ The ELNES obtained from the screw dislocation exhibits visible differences compared to the bulk. Similar to our observation in the $(a/2)[110]$ partial dislocation core,¹⁶ a decrease of the e_g/t_{2g} ratio was found compared to the bulk. Since the loss of oxygen leads to a reduced crystal field, this result is contrary to van der Laan and Kirkman³⁰ who calculated an increase of the e_g/t_{2g} ratio if the crystal field is reduced. On the other hand, the narrowing of the e_g and t_{2g} peaks as well as the increase of the L_3/L_2 ratio are in accordance with a reduction of the crystal field at the Ti sites in the core. There will certainly also be a contribution from the distortion of the TiO₆ octahedra in the core which occurs in the displacement field of any dislocation. Our results seem to coincide with the observations by Klie and Browning,⁸ who reported that the L_3/L_2 ratio in grain boundaries of SrTiO₃ in the heating cycle is invariably increased compared to the bulk.

V. SUMMARY AND CONCLUSION

The $a\langle 100 \rangle$ screw dislocation core has been studied by means of HRTEM and EELS. The displacement field around the core does not correspond to that obtained from linear anisotropic elasticity theory. Some additional weak contrast is present in the HRTEM images. Strain mapping reveals that the core is slightly expanded, particularly along $\langle 110 \rangle$ directions. We concluded that this effect does not come only from surface relaxations, which was confirmed by image simulations. Rather, the EELS results show that changes of the chemistry and Ti coordination lead to a reconstruction of the core with small $\langle 110 \rangle$ edge components.

Atomistic simulations of defects in SrTiO₃ are clearly desirable. However, considerable difficulties arise owing to the fact that SrTiO₃ is partly ionic, which leads to charges which are difficult to balance out.

ACKNOWLEDGMENTS

We are indebted to M. Mrovec and C. Elsässer for helpful discussions. One of the authors (Z.L.Z.) is grateful for support from the Max-Planck Society. We would like to thank Professor Manfred Rühle for his encouragement and stimulating discussions. We also thank M. Sycha for the excellent TEM specimen preparation and Dr. K. Du and Dr. F. Phillipp for helpful discussions with the image processing and simulation.

- ¹J. Verbeeck, O. I. Lebedev, and G. van Tendeloo, *Phys. Rev. B* **66**, 184426 (2002); M. J. Dalberth, R. E. Stauber, J. C. Price, C. T. Rogers, and D. Galt, *Appl. Phys. Lett.* **72**, 507 (1998).
- ²O. Kienzle, M. Exner, and F. Ernst, *Phys. Status Solidi A* **166**, 57 (1998).
- ³S. Hutt, S. Köstlmeier, and C. Elsässer, *J. Phys.: Condens. Matter* **13**, 3949 (2001).
- ⁴S.-D. Mo, W. Y. Ching, M. F. Chisholm, and G. Duscher, *Phys. Rev. B* **60**, 2416 (1999).
- ⁵N. D. Browning, S. J. Pennycook, M. F. Chisholm, M. M. McGibbon, and A. J. McGibbon, *Interface Sci.* **2**, 397 (1995).
- ⁶M. M. McGibbon, N. D. Browning, M. F. Chisholm, A. J. McGibbon, S. J. Pennycook, V. Ravikumar, and V. P. Dravid, *Science* **266**, 102 (1994).
- ⁷R. F. Klie, Y. Ito, S. Stemmer, and N. D. Browning, *Ultramicroscopy* **86**, 289 (2001).
- ⁸R. F. Klie and N. D. Browning, *Defect Diffus. Forum* **206-2**, 31 (2002).
- ⁹J. Nishigaki, K. Kuroda, and H. Saka, *Phys. Status Solidi A* **128**, 319 (1991).
- ¹⁰Z. Mao and K. M. Knowles, *Philos. Mag. A* **73**, 699 (1996).
- ¹¹T. Matsunaga and H. Saka, *Philos. Mag. Lett.* **80**, 597 (2000).
- ¹²Y. L. Qin, C. L. Jia, J. H. Hao, X. X. Xi, and K. Urban, *J. Mater. Res.* **17**, 3117 (2002).
- ¹³P. Gumbsch, S. Taeri-Baghdarani, D. Brunner, W. Sigle, and M. Rühle, *Phys. Rev. Lett.* **87**, 085505 (2001).
- ¹⁴R. A. de Souza, J. Fleig, J. Maier, O. Kienzle, Z. L. Zhang, W. Sigle, and M. Rühle, *J. Am. Ceram. Soc.* **86**, 922 (2003).
- ¹⁵Z. L. Zhang, W. Sigle, and M. Rühle, *Phys. Rev. B* **66**, 094108 (2002).
- ¹⁶Z. L. Zhang, W. Sigle, W. Kurtz, and M. Rühle, *Phys. Rev. B* **66**, 214112 (2002).
- ¹⁷Y. Xin, S. J. Pennycook, N. D. Browning, P. D. Nellist, S. Sivanathan, F. Ommes, B. Beaumont, J. P. Faurie, and P. Gibart, *Appl. Phys. Lett.* **72**, 2680 (1998); J. E. Northrup, *ibid.* **78**, 2288 (2001).
- ¹⁸J. W. P. Hsu, M. J. Manfra, D. V. Lang, S. Richter, S. N. G. Chu, A. M. Sergent, R. N. Kleiman, and L. N. Pfeiffer, *Appl. Phys. Lett.* **78**, 1685 (2001).
- ¹⁹W. Sigle, *Philos. Mag. A* **79**, 1009 (1999).
- ²⁰S. Ismail-Beigi and T. A. Arias, *Phys. Rev. Lett.* **84**, 1499 (2000).
- ²¹T. J. Balk and K. J. Hemker, *Philos. Mag. A* **81**, 1507 (2001).
- ²²T. J. Balk and K. J. Hemker, *Mater. Sci. Eng., A* **309-310**, 108 (2001).
- ²³W. Kurtz, *Z. Metallkd.* **93**, 432 (2002).
- ²⁴H. F. Fischmeister, G. Elßner, B. Gibbesch, K.-H. Kadow, F. Kawa, D. Korn, W. Mader, and M. Turwitt, *Rev. Sci. Instrum.* **64**, 234 (1993).
- ²⁵P. Stadelmann, *Ultramicroscopy* **21**, 131 (1987).
- ²⁶K. Du, Y. Rau, N. Y. Jin-Phillipp, and F. Phillipp, *J. Mater. Sci. Technol.* **18**, 135 (2002).
- ²⁷H. Müllejjans and J. Bruley, *J. Microsc.* **180**, 12 (1995).
- ²⁸C. Scheu, W. Stein, and M. Rühle, *Phys. Status Solidi B* **222**, 199 (2000).
- ²⁹D. H. Pearson, C. C. Ahn, and B. Fultz, *Phys. Rev. B* **47**, 8471 (1993).
- ³⁰G. van der Laan and I. W. Kirkman, *J. Phys.: Condens. Matter* **4**, 4189 (1992).